Available online at www.sciencedirect.com
ScienceDirect
Journal of Molecular Catalysis A: Chemical 274 (2007) 159–168
JOURNAL OF MOLECULAR CATALYSIS A: CHEMICAL
www.elsevier.com/locate/molcata

Propene epoxidation by nitrous oxide over Au–Cu/TiO_2 alloy catalysts

R.J. Chimentão [a], F. Medina [a,*], J.L.G. Fierro [b], J. Llorca [c], J.E. Sueiras [a], Y. Cesteros [d], P. Salagre [d]

[a] *Dept. d'Enginyeria Química, Universitat Rovira i Virgili, Tarragona 43007, Spain*
[b] *Instituto de Catálisis y Petroleoquímica, CSIC, Cantoblanco, Madrid 28049, Spain*
[c] *Institut de Tècniques Energètiques, Universitat Politècnica de Catalunya, Diagonal 647, ed. ETSEIB, Barcelona 08028, Spain*
[d] *Dept. de Química Inorgánica, Universitat Rovira i Virgili, Tarragona 43007, Spain*

Received 5 April 2007; received in revised form 3 May 2007; accepted 4 May 2007
Available online 13 May 2007

Abstract

Gold–copper alloy catalysts were prepared by impregnation of TiO_2 (anatase) support with mixed chloride precursors and tested in the gas-phase epoxidation of propene. The bimetallic systems contained different Au–Cu molar ratios and a total metal content of 4 wt.%. The corresponding monometallic Au/TiO_2 and Cu/TiO_2 catalysts were also prepared for comparison. X-ray diffraction, XPS and transmission electron microscopy studies indicated that alloying was achieved. The copper content in the catalyst seemed to have a strong influence on the dispersion and catalytic properties of the metal particles. In particular, the greater the Cu content in the alloy, the smaller the metal particle. These changes also contributed to an increase in activity and selectivity to propene oxide. The sample with a Cu/Au ratio of 3/1 showed the best catalytic behaviour. Moreover, the catalytic activity of the samples can be correlated with the results obtained by TPR.

Keywords: Alloy; Gold; Copper; Propene; Epoxidation; Catalysts; Nitrous oxide; HRTEM; XPS

1. Introduction

Propene oxide (PO) is one of the most important chemical feedstocks for producing resins such as polyurethane [1–3]. Conventional manufacturing methods require a two-stage process that uses chlorohydrin or Halcon (hydroperoxides) as an oxidant. The process with chlorohydrin method consumes large amounts of Cl_2, which causes serious problems such as equipment corrosion and environmental pollution. The method with Halcon is capital intensive and its viability depends on the economic fortunes of the byproducts, namely styrene or tert-butyl-alcohol. In analogy to ethylene epoxidation, much attention has been paid to the direct oxidation of propene using air or oxygen directly as the oxidant [4]. The epoxidation of ethylene with gaseous oxygen over Ag catalysts was developed many years ago, but the same reaction with propene has not been successful. Propene is different from ethylene in the existence of a methyl group. It is generally believed that this low efficiency of propene epoxidation is associated with the presence of allylic hydrogen atoms in the alkene, which readily undergo abstraction on oxygenated silver to yield a stable adsorbed allyl species precluding selective oxidation, thus, leading to combustion. Haruta and co-workers [5] reported that certain Au/TiO_2 catalysts exhibit a selectivity of over 90% for the production of propene oxide (PO) using a combination of H_2 and O_2 as oxidation mixture, though the reactant conversion was very low (1.1%). When formed as particles of less than 10 nm and supported on metal oxides, Au is an active catalyst with unusual size-dependent activity and selectivity for propene epoxidation [6,7]. For active supports such as TiO_2, the oxygen activation occurred on the support surface and the oxidation reaction occurred at the periphery between the support and the gold nanoparticles. The requirement for very small metal nanoparticles may, therefore, arise mainly from larger contact peripherals. The preparation route of gold catalysts has also been shown to be particularly important for propene epoxidation. Among single metal oxides, TiO_2 makes Au selective for propene epoxidation only in the anatase form [8]. Another constraint is the deactivation of gold catalysts with time on stream [9]. The accumulation of PO and other successively oxidized products on the catalyst surfaces was con-

* Corresponding author.
E-mail address: francesc.medina@urv.cat (F. Medina).

1381-1169/$ – see front matter © 2007 Elsevier B.V. All rights reserved.
doi:10.1016/j.molcata.2007.05.008

sidered to be a main reason for this phenomenon and for the limited propene conversion. Recently, Lambert and co-workers have shown that copper is also extremely effective in the epoxidation of propene [10]. It is interesting, therefore, to examine how copper and gold alloy catalysts behave in propene epoxidation. The structure of bulk Au–Cu alloy is well-known and this alloy is known to form solid solution very easily. The main aim of this study is to explore the performance of Au–Cu alloy in the epoxidation of propene by nitrous oxide (N_2O). The decomposition of N_2O is expected to generate oxygen species with an electrophilic characteristic on a suitable catalyst, which may account for the highly selective epoxidation of propene [11,12]. The only byproduct is N_2, so the process using N_2O as oxidant is environmentally benign. In this study several Au–Cu bimetallic catalysts as well as monometallic Cu and Au ones were prepared. The materials were characterized by N_2-adsorption, TPR, XRD, HRTEM, EELS and XPS. The role of copper on Au dispersion and the catalytic properties were assessed. This provided relevant structure-function relationships for the investigated reaction over a novel catalytic system.

2. Experimental

2.1. Catalyst preparation

Gold–copper alloy catalysts supported on titanium oxide were prepared. Since gold is miscible with copper at any composition range, this covered the entire composition. The Au–Cu/TiO_2 catalysts were prepared by impregnating the support (TiO_2, anatase) with an acidic aqueous solution of $HAuCl_4 \cdot 3H_2O$ and $CuCl_2 \cdot H_2O$ in sufficient amounts. The samples were dried for 2 h in vacuum. The resulting samples were then dried for 12 h at 373 K and finally reduced in a hydrogen flow (50 mL min^{-1}) for 6 h at 673 K. The total metal loading of all samples (monometallic and bimetallic samples) was fixed at 4 wt.%. The Au/Cu molar ratios in bimetallic samples were 3/1, 1/1 and 1/3. A monometallic gold sample with 0.5 wt.% of gold was also prepared in order to study how the amount of gold and the size of metal particle affect catalytic behaviour.

The sample code of the bimetallic catalysts refers to the molar ratios (e.g. Au_3Cu_1).

2.2. Catalyst characterization

2.2.1. N_2 physisorption

N_2-adsorption–desorption isotherms at 77 K were measured in a Micromeritics ASAP 2000 instrument. Samples were previously evacuated at 623 K for 16 h. The BET method was used to calculate the total surface area of the samples [13]. The BET surface areas of the samples were around 28–31 $m^2\ g^{-1}$, which is quite similar to that of the support (31 $m^2\ g^{-1}$).

2.2.2. Temperature-programmed reduction (TPR)

TPR experiments were performed in a TPDRO 1100 (Thermo Finnigan) instrument equipped with a thermal conductivity detector (TCD) and coupled to a mass spectrometer QMS 422 Omnistar. The catalysts were treated in O_2 for 1 h at 623 K before TPR analysis. The samples were then purged with argon flow before the TPR analysis. The TPR of the catalysts was carried out using 5% H_2 in Ar flow as reducing agent. The gas flow rate was 20 mL min^{-1} and the weight of sample was around 30 mg. The temperature was raised from 323 to 1073 K at a rate of 20 K min^{-1}. Water produced during TPR was trapped in $CaO + Na_2O$ (Soda lime).

2.2.3. X-ray diffraction

X-ray diffraction (XRD) measurements were taken using a Siemens D5000 diffractometer (Bragg–Bentano parafocusing geometry and vertical θ–θ goniometer) fitted with a grazing incident (ω: 0.52°) attachment for thin film analysis and scintillation counter as a detector. The samples were dispersed on Si (5 1 0) sample holder. The angular 2θ diffraction range was between 10° and 120°. The data were collected with an angular step of 0.03° at 12 s per step and sample rotation. Cu Kα radiation ($\lambda = 1.54056$ Å) was obtained from a copper X-ray tube operated at 40 kV and 30 mA. The crystalline phases were identified using the JCPDS files.

2.2.4. Transmission electron microscopy (TEM)

Transmission electron microscopy studies were performed at 200 kV with a JEOL JEM 2010F instrument equipped with a field emission source and an electron energy-loss spectroscopy (EELS) detector. The microscope was operated in high-resolution (HRTEM) and scanning (STEM) modes, both in bright-field and dark-field configurations. Samples were dispersed in alcohol in an ultrasonic bath and a drop of supernatant suspension was poured onto a holey carbon-coated grid and dried completely before the measurements were taken.

2.2.5. X-ray photoelectron spectroscopy (XPS)

X-ray photoelectron spectra (XPS) were acquired with a VG Escalab 200R spectrometer equipped with a hemispherical electron analyzer and an Mg Kα ($h\nu = 1253.6$ eV, $1\ eV = 1.603 \times 10^{-19}$ J). The X-ray source operated at 10 mA and 12 kV. The peaks were fitted by a non-linear least square fitting program using a properly weighted sum of Lorentzian and Gaussian component curves after background subtraction according to Briggs and Seah [14]. The constant charging of the samples was corrected by referencing all energies to the Al 2p peak at 74.5 eV.

2.2.6. Catalytic activity

The catalytic reactions were carried out using a fixed-bed reactor operated at atmospheric pressure. The experiments were typically carried out with 0.14 g of catalyst and a gas flow of 50 NmL min^{-1} (GHSV 9000 h^{-1}). The gas mixture consisted of 10% of N_2O and 10% propene in argon. Before the reaction, the catalysts were pretreated with a gas flow containing Ar (100 mL min^{-1}) and H_2 (10 mL min^{-1}) at 673 K for 2 h. After the temperature was decreased to the desired reaction temperature, the reactant gas mixture of Ar, C_3H_6 and N_2O was introduced to start the reaction. The products were analyzed by two on-line gas chromatographs equipped with Porapak T and molecular sieve columns using FID and TCD detectors. All

lines and valves between the exit of the reactor and the gas chromatographs were heated at 373 K to prevent the condensation of the products.

3. Results and discussion

3.1. Catalysts characterization

3.1.1. XRD

X-ray diffraction of all samples was conducted to ensure that, with the preparation procedure adopted in this study, alloying had been obtained in the bimetallic formulations. The XRD patterns in Fig. 1 show broad peaks due to the anatase support (JCPDS 211272). For 4%Au/TiO_2 and 0.5%Au/TiO_2 samples, diffraction lines of gold were identified at 38.2°, 44.3°, 64.5° and 77.6°, which we assigned to the (1 1 1), (2 0 0), (2 2 0), (3 1 1) planes of the fcc structure of gold, respectively (JPCDS 04-0784). Typical XRD of the Cu sample (Cu/TiO_2) showed 2θ values at 43.4°, 50.6° and 74.2°, which are indexed as (1 1 1), (2 0 0) and (2 2 0) planes of the fcc structure of copper (JCPDS file, 4–386). Other phases, such as CuO and Cu_2O, were not detected. This means that, if part of the copper exists in the form of copper oxide clusters, these are under the detection capabilities of XRD [15]. In the bimetallic samples, broad diffraction lines corresponding to (1 1 1) planes of Au–Cu alloys were identified, whereas (2 0 0) and (2 2 0) Bragg reflections became hardly visible due to peak broadening. This effect is more pronounced as the copper content increases in sample formulation. The mean particle diameter calculated from the (1 1 1) reflection by the Scherrer formula for the 4%Au/TiO_2, 0.5%Au/TiO_2, 4%Au_3Cu_1/TiO_2, 4%Au_1Cu_1/TiO_2, 4%Au_1Cu_3/TiO_2 and 4%Cu/TiO_2 samples are Au = 27.1 nm, Au = 8.6 nm, Au_3Cu_1 = 13.5 nm, Au_1Cu_1 = 9.3 nm, Au_1Cu_3 = 7.3 nm and Cu = 5.5 nm, respectively. For pure gold samples, when the amount of gold decreased from 4 to 0.5%, the gold particle size decreased from 27.1 to 8.6 nm. For bimetallic catalysts, on the other hand, when the copper content increased the bimetallic particles size decreased. The pure monometallic copper catalyst showed the lowest metal particle size (5.5 nm). When gold and copper are brought together to form a solid, the electronic charge density is compressed [16]. This may contribute to the fact that the as-synthesized bimetallic particles are more stable against agglomeration than pure elements. The formation of alloys in the bimetallic samples is demonstrated by the $d_{1\,1\,1}$ values, which progressively decreased as the Cu content decreased in relation to pure Au. Fig. 2 shows the lattice parameters of the metal crystallites in our samples as a function of bulk composition. When the copper content increased from a Cu/Au molar ratio of 1/3 to 3/1, the lattice parameter gradually decreased. A linear evolution of the lattice parameter of the Au–Cu crystallites. Therefore, clearly indicates the formation of alloys in the bimetallic samples. However, in agreement with previous studies, the lattice parameters of our bimetallic samples exhibit several small deviations of Vegard's law [17].

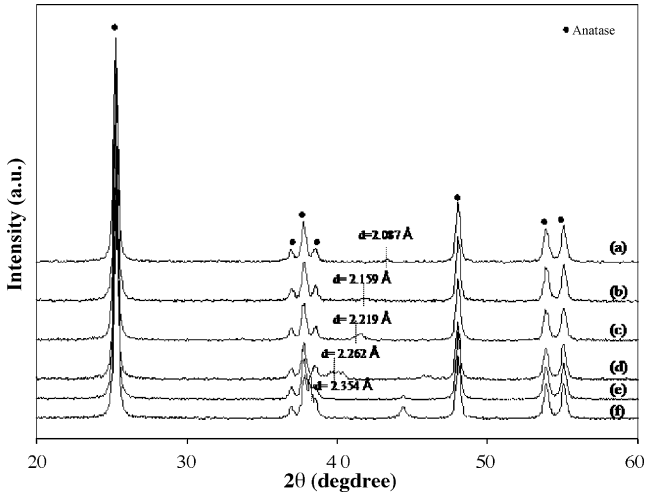

Fig. 1. XRD patterns of Au, Cu and Au–Cu alloys supported on TiO_2: (a) 4%Cu/TiO_2, (b) 4%Au_1Cu_3/TiO_2, (c) 4%Au_1Cu_1/TiO_2, (d) 4%Au_3Cu_1/TiO_2, (e) 0.5%Au/TiO_2 and (f) 4%Au/TiO_2.

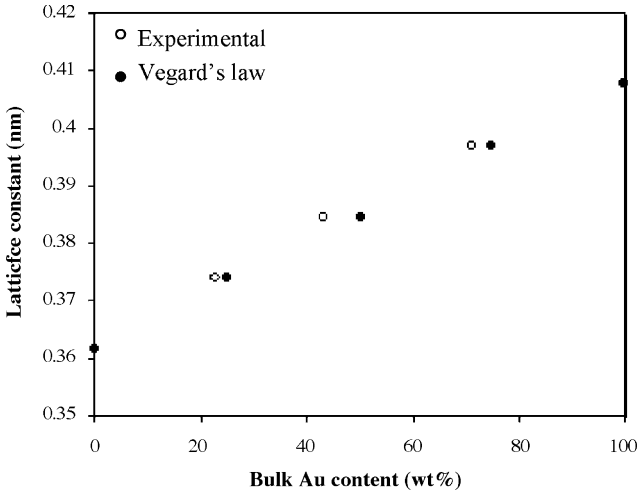

Fig. 2. Effect of Au–Cu composition on the lattice parameter, a_0, of fcc alloy crystallites calculated from the (1 1 1) crystallographic plane by XRD.

3.1.2. TEM

To obtain further insight into the nature of the metal and alloy particles identified by XRD, we conducted a detailed TEM–EELS study of all the catalysts. The 4%Au/TiO_2 catalyst is made up of small metal particles ranging from 8 to 15 nm in diameter and of large agglomerates of up to 100–250 nm. This is shown in Fig. 3, where the location of gold particles and agglomerates are seen in the same area taken in bright-field (BF) and dark-field (DF) modes. This indicates that the size distribution of Au particles in this sample is quite heterogeneous and that the agglomeration of Au occurs easily. In contrast, the monometallic catalyst 4%Cu/TiO_2 is mainly made up of copper metal particles of between 10 and 20 nm in diameter. Similarly, all the bimetallic samples and the 0.5%Au/TiO_2 sample are made up of only well-dispersed metallic particles at the nanometer scale. Fig. 4 shows a representative image of a metallic particle in the catalyst 4%Au_3Cu_1/TiO_2 catalyst obtained under Z-contrast, BF and DF STEM modes. All particles imaged in this catalyst had diameters of about 15–25 nm. High-resolution TEM (HRTEM)

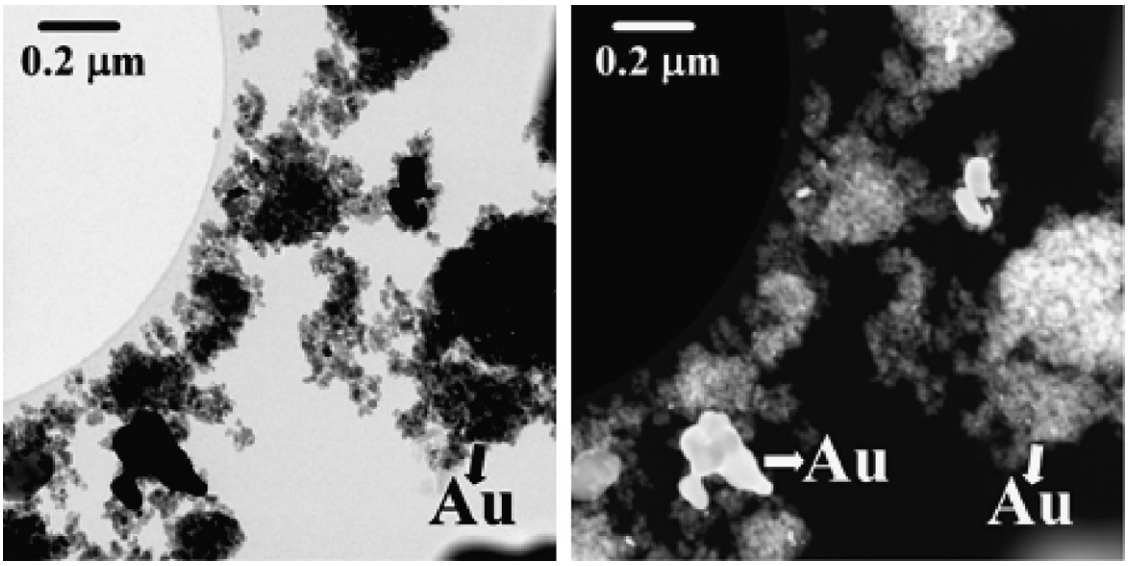

Fig. 3. Bright-field (left) and dark-field (right) TEM images of catalyst 4%Au/TiO_2 at low magnification. In the DF image, individual gold particles as well as gold agglomerates appear bright.

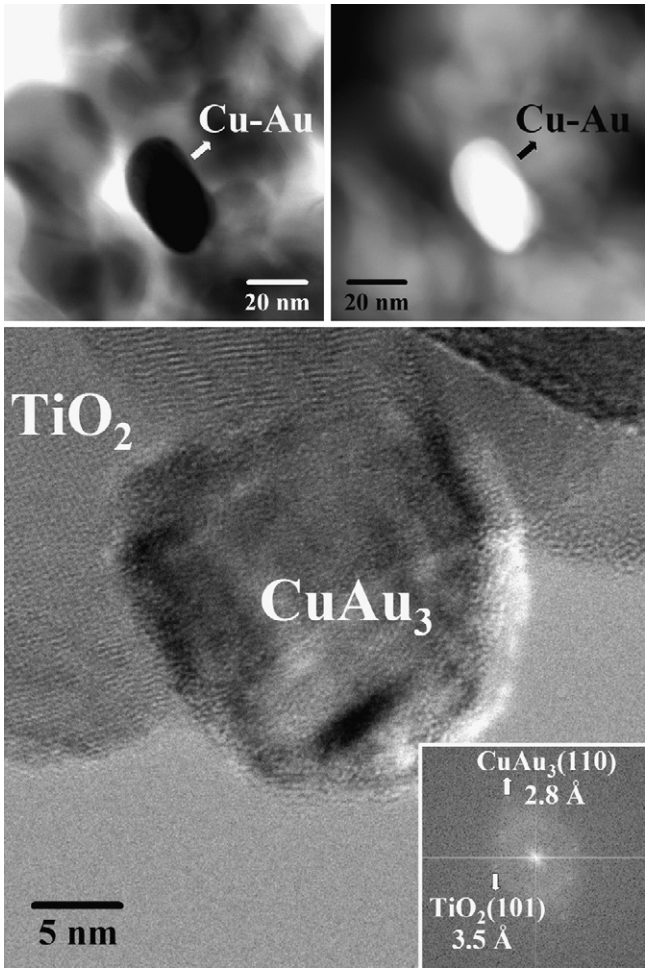

Fig. 4. Z-contrast STEM, HRTEM and FT images of individual metal particles in catalyst 4%Au_3Cu_1/TiO_2. EELS analysis reveal that particles are bimetallic, and lattice-fringe and FT analysis show Cu_1Au_3 particles supported on TiO_2.

and electron energy-loss spectroscopy (EELS) were performed over individual particles. In all cases, EELS data revealed the simultaneous presence of gold and copper for each individual metallic particle analyzed and HRTEM revealed the presence of the Au_3Cu_1 alloy (Fig. 4). Particles in the 4%Au_1Cu_1/TiO_2 catalyst exhibited a narrow size distribution of about 5–10 nm. Fig. 5 shows STEM images for this catalyst as well as EEL spectra recorded over different areas. The area labeled "a" in the figure, with low Z-contrast, correspond to the TiO_2 support according to EELS (characteristic pattern with peaks at about 5, 11, 23, 38 and 46 eV). The area labeled "b" depicts a particle with high Z-contrast and an EEL spectrum that indicates a bimetallic Cu–Au composition (a single signal at ca. 25 eV). Another individual particle in the Au_1Cu_1/TiO_2 catalyst is shown in Fig. 6 in BF and DF STEM modes as well as under HRTEM conditions. The atomic-scale image along with FT indicates that the particle corresponds to the Cu–Au alloy. All the lattice-fringe images recorded over metallic particles in the 4%Au_1Cu_1/TiO_2 catalyst corresponded to the Au–Cu alloy and no other alloys in the Au–Cu system were identified. Fig. 7 corresponds to STEM images of a representative particle in the 4%Au_1Cu_3/TiO_2 catalyst. In this catalyst, the size of the particles ranged from 10 to 15 nm. Again, EELS data demonstrated the bimetallic composition of particles and, in this case, HRTEM analysis identified Au_1Cu_3 crystallites located on the top TiO_2 crystals of the support (Fig. 7).

3.1.3. TPR

TPR profiles recorded over 4%Au–Cu alloy catalysts of several compositions and over 4%Au/TiO_2 and 4%Cu/TiO_2 samples are shown in Fig. 8a. The TPR profile for the Cu/TiO_2 sample presented two reduction peaks centred at 460 and 630 K, which can be ascribed as highly dispersed Cu(II)O clusters and the isolated Cu(II) ions, respectively [18–20]. Similarly, two TPR peaks were recorded over all catalysts with Au–Cu alloys, as shown in Fig. 8a, but their position and absolute intensity

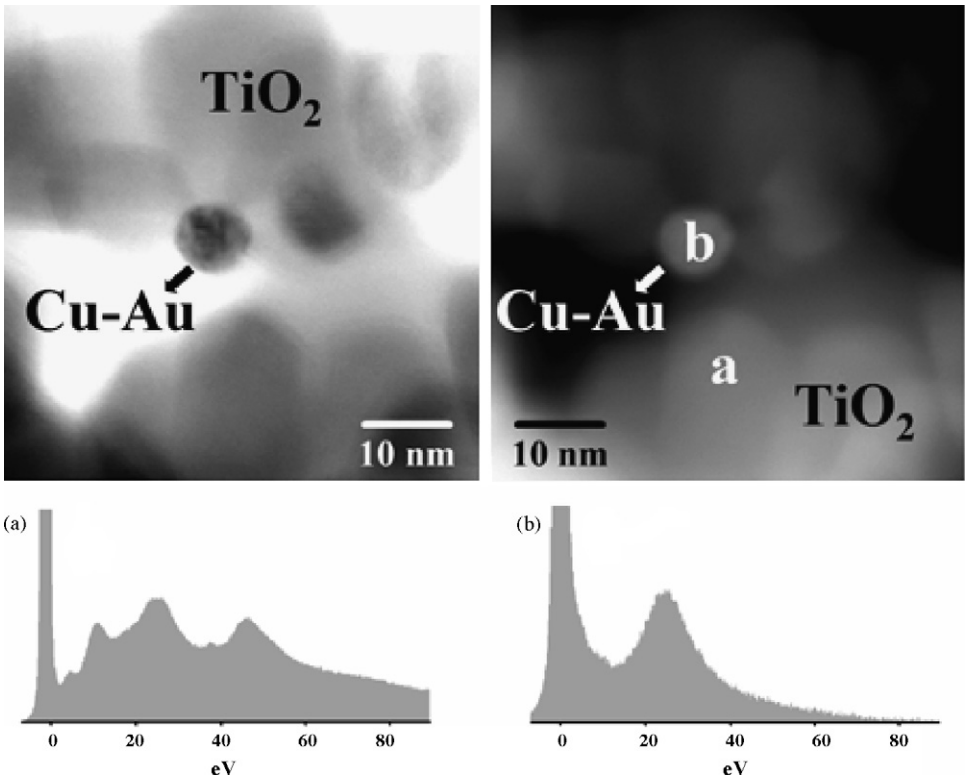

Fig. 5. Z-contrast STEM images of catalyst 4%Au_1Cu_1/TiO_2 and EEL spectra recorded over areas marked as "a" (corresponding to TiO_2) and "b" (bimetallic Cu–Au particle).

depended on the composition of the alloy particles. Both the low temperature and high temperature TPR peaks of the bimetallic samples shift to lower values as the Cu content increases. The maximum of the low temperature peak varied from ca. 470 K for the 4%Au_3Cu_1/TiO_2 catalyst to around 440 K for the 4%Au_1Cu_1/TiO_2 and 4%Au_1Cu_3/TiO_2 catalysts. The high temperature peak shifted from 650 K for 4%Au_1Cu_1/TiO_2 to 630 K for 4%Cu/TiO_2. This may be because copper atoms can affect the electronic structure of gold by near-neighbour interactions [21]. The work function of Cu is reported to be 4.65 eV, while that of gold is 5.1 eV. Since the work function of copper is lower than that of gold, electronic interactions between Au and Cu atoms are expected to result in electron transfer from copper to gold, which in turn leads to a lower reduction temperature. Also, as the size of the bimetallic particle decreased as the copper content decreased, as is confirmed by XRD and HRTEM results, obviously the fraction of the surface atoms also increased. At the same time, because the overlap of electron orbitals decreases as the average number of bonds between atoms decreases, the band structure is weakened and the surface atoms in particular start to behave more as individuals than as members of the cluster [22]. This could also explain the shift towards lower temperatures observed in the TPR when the Cu content increased. Another important fact must also be considered, for the bimetallic samples, and particularly for the 4%Au_1Cu_1/TiO_2 and 4%Au_1Cu_3/TiO_2 samples, the low temperature peak increased in intensity and the high temperature peaks decreased (see Fig. 8b and c, respectively). Fig. 8b clearly shows that the low temperature TPR peaks in the 4%Au_1Cu_1/TiO_2 and 4%Au_1Cu_3/TiO_2 catalysts are significantly more intense than those of the other samples. The H_2 consumption observed for our bimetallic samples was higher than was theoretically expected. The discrepancy between theoretical and experimental values can be tentatively explained by the reduction of the support surface upon hydrogen spillover. Copper may act as a dispersant agent for gold that decreases the bimetallic particle size of clusters, as is confirmed by our XRD and HRTEM analysis. This increases the dissociative adsorption of hydrogen on such metal sites to the adjacent support sites. Previous work on the activation of hydrogen in Au/TiO_2 catalysts showed that H_2 dissociates on nanosized gold to produce the reduction in the support by spillover [23]. This may also explain the low H_2 uptake observed for the monometallic 4%Au/TiO_2, since these larger gold particles do not adsorb H_2 to any appreciable extent. This is an important distinctive behaviour among catalysts and may strongly influence catalytic performance. The greater reducibility of 4%Au_1Cu_1/TiO_2 and 4%Au_1Cu_3/TiO_2 catalysts may be related to the lower particle size in relation to that of other samples (as proven by XRD and TEM results) and to geometric effects in the alloy particles [24]. This also suggests that hydrogen adsorption is dependent on particle size. Finally, further evidence of a strong alloying-derived effect in these samples is the appearance of a low-intense, intermediate TPR peak at ca. 555 K.

3.1.4. XPS

XPS is a powerful technique that provides valuable information about the chemical compositions of nanoparticles [25,26].

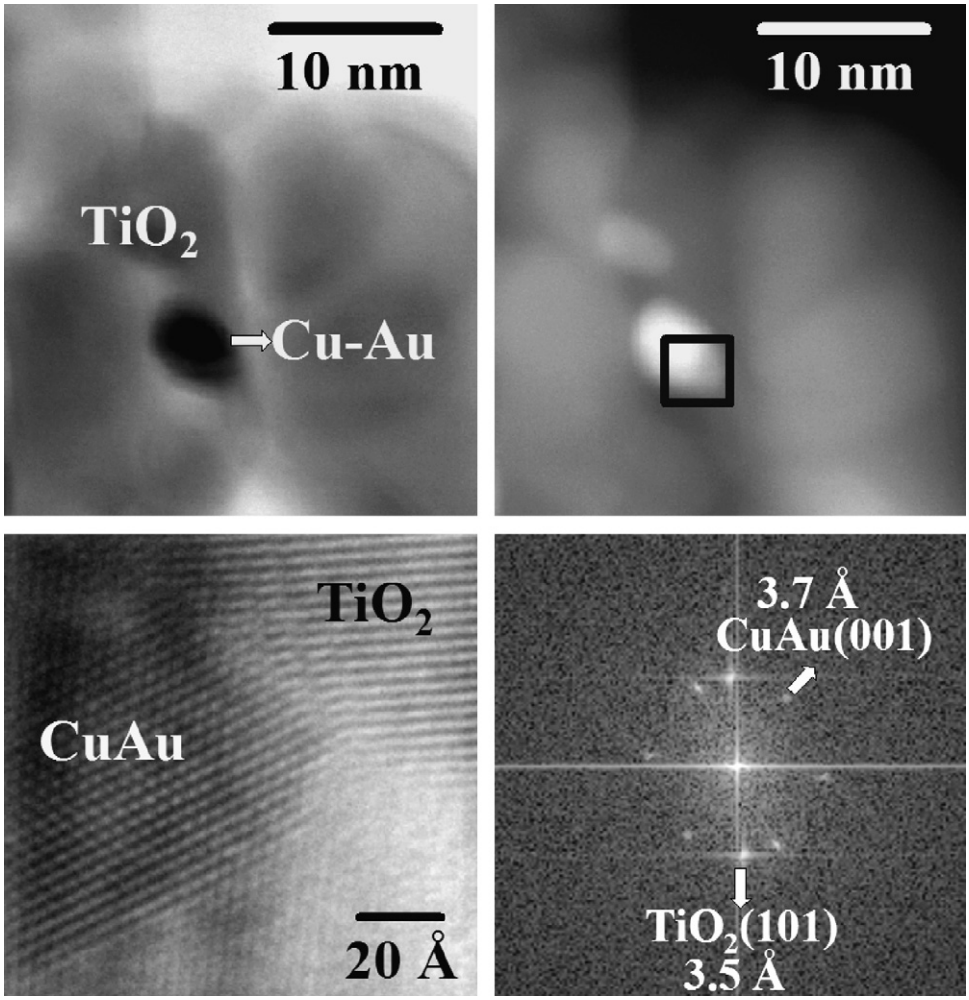

Fig. 6. Z-contrast STEM images of an individual metal particle in catalyst 4%Au_1Cu_1/TiO_2 and HRTEM and FT images corresponding to the area enclosed by the square. The lattice-fringe analysis indicates that the particle is Cu–Au alloy.

For this reason we performed surface analysis by XPS. Table 1 summarizes the elemental XPS positions and the atomic ratios of Cu/Ti and Au/Ti. The binding energy of the Ti $2p_{3/2}$ peak at 458.7 eV was unchanged for all samples. The corresponding XPS core level spectra acquired for the Au 4f and Cu 2p regions are shown in Fig. 9. For the 4%Au/TiO_2 sample, the Au 4f spectra, characterized by spin-orbit splitting (Au $4f_{7/2}$ and Au $4f_{5/2}$ components), shows values of 84.0 and 87.7 eV, respectively. Both peaks originating from the Au indicate that these binding energies are consistent with the Au^0 oxidation state. The Au $4f_{7/2}$ binding energies obtained from the bimetallic samples were in the 83.7–83.8 eV range. As the copper content in the bimetallic catalysts increased, the binding energy of the Au $4f_{7/2}$ shifted towards lower binding energies than in the monometallic gold sample. According to Pauling's eletronegativity table, Au is more electronegative than Cu. We should, therefore, expect some electron transfer from copper to gold atoms by the shifting of Au core levels towards lower binding energies [27]. Although the shift in binding energy of Au $4f_{7/2}$ core level in the bimetallic systems with respect to that of Au/TiO_2 one is small, it is somewhat larger than the error of measurements (±0.1 eV). Thus, it can be reasonably assumed that electron transfer from copper to gold is taking place. The shift of the Au $4f_{7/2}$ to the lower energies observed for our samples containing alloy particles is consistent with this general rule. No evidence of Au bonded to oxygen was encountered

Table 1
Binding energies (eV) and surface atomic ratios of TiO_2-supported Au–Cu catalysts

Catalyst	Ti $2p_{3/2}$	Cu $2p_{3/2}$	Au $4f_{7/2}$	Au/Ti atomic ratio	Cu/Ti atomic ratio
4%Cu/TiO_2	458.7	932.3	–	–	0.064
4%Au_3Cu_1/TiO_2	458.7	932.2	83.8	0.0089	0.012
4%Au_1Cu_1/TiO_2	458.7	932.2	83.7	0.0083	0.022
4%Au_1Cu_3/TiO_2	458.7	932.5	83.7	0.0030	0.040
4%Au/TiO_2	458.7	–	84.0	0.0068	–

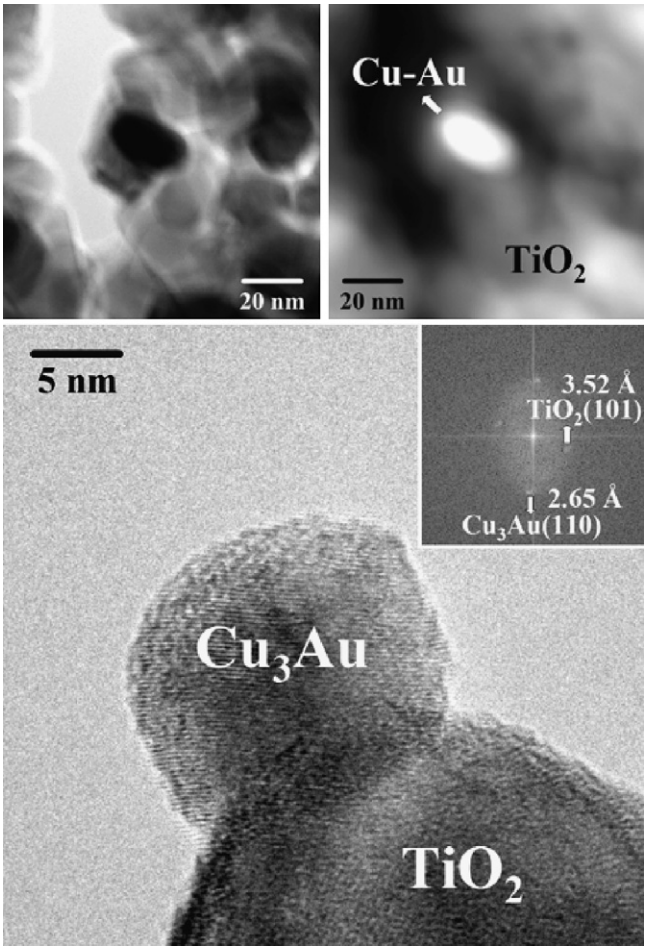

Fig. 7. Z-contrast STEM, HRTEM and FT images of individual metal particles in catalyst 4%Au_1Cu_3/TiO_2. EELS analysis indicates that particles are bimetallic, and lattice-fringe and FT analysis correspond to Cu_3Au particles supported on TiO_2.

because the oxide shows binding energies of around 85.8 and 89.5 eV for Au $4f_{7/2}$ and Au $4f_{5/2}$, respectively [28–30]. With regard to copper, as the Au content in the bimetallic samples increased, the binding energies of Cu $2p_{3/2}$ slightly shifted to higher energy values than those of the monometallic copper sample. The higher electron affinity of gold with respect to that of copper led to an electron transfer from the Cu to Au, thus, decreasing the electron density of the Cu atoms. In all cases the Cu $2p_{3/2}$ values were found to be between 932.2 and 932.5 eV, which is about 1.5 eV lower than for CuO, which, thus, precludes the form of CuO. From the relative surface atomic ratios (Au/Ti and Cu/Ti) in Table 1, it is interesting how the state of dispersion of the bimetallic samples was affected by the addition of copper. For example, 4%Au_1Cu_1/TiO_2 shows an Au/Ti ratio of 0.0083, while the Au/Ti ratio for monometallic gold catalysts is 0.0068. Taking into account the amount of gold in these samples, therefore, we can conclude that adding copper significantly increases the dispersion of the bimetallic samples. This effect was not observed for copper, however, which suggests that the particle size of our pure copper catalysts is quite similar to that of the bimetallic samples, as was confirmed by XRD and HRTEM.

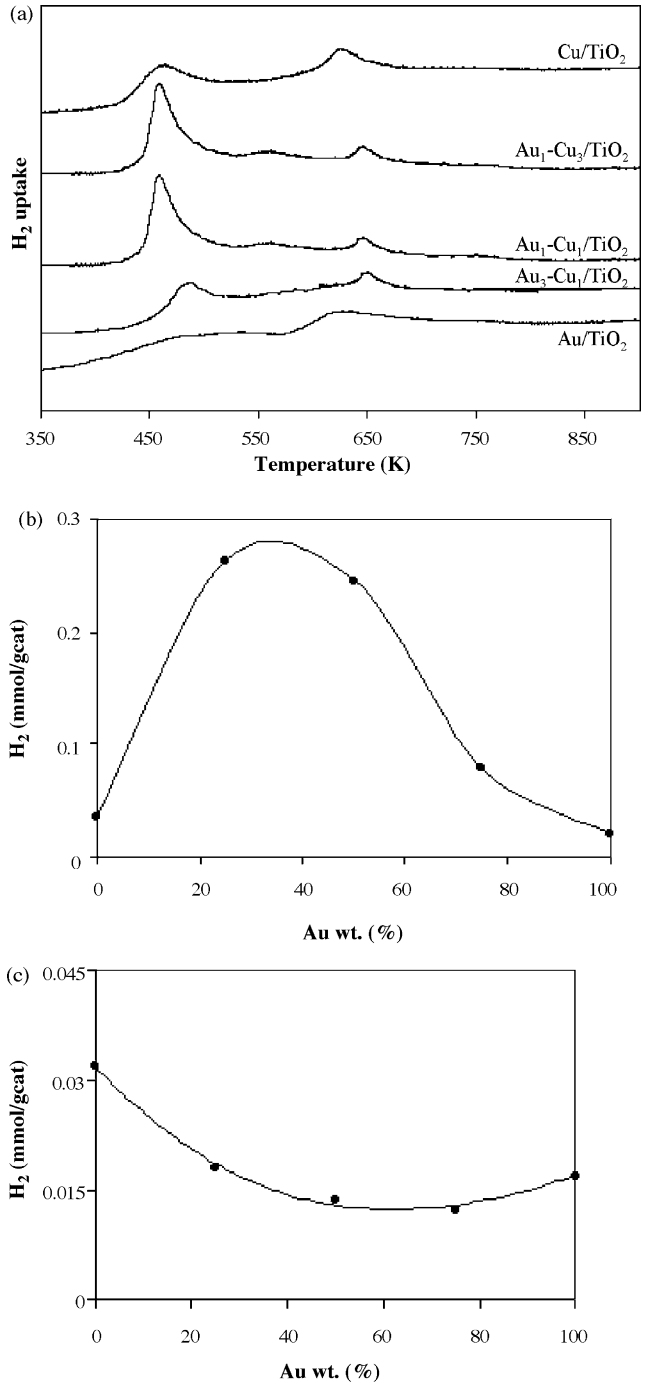

Fig. 8. (a) TPR profiles of 4%Cu/TiO_2, 4%Au/TiO_2 and 4%Au–Cu/TiO_2 catalysts. Amount of hydrogen uptake: (b) low temperature and (c) high temperature peak.

3.2. Catalytic activity

The direct propene epoxidation reaction with N_2O was tested at several reaction temperatures (between 530 and 653 K). The main products obtained were acrolein, acetone, propanal, propene oxide and total combustion products (H_2O and CO_x). In a blank experiment it was determined that TiO_2 alone had no activity for the epoxidation of propene with N_2O in the range of temperatures tested. To see whether consecutive reactions

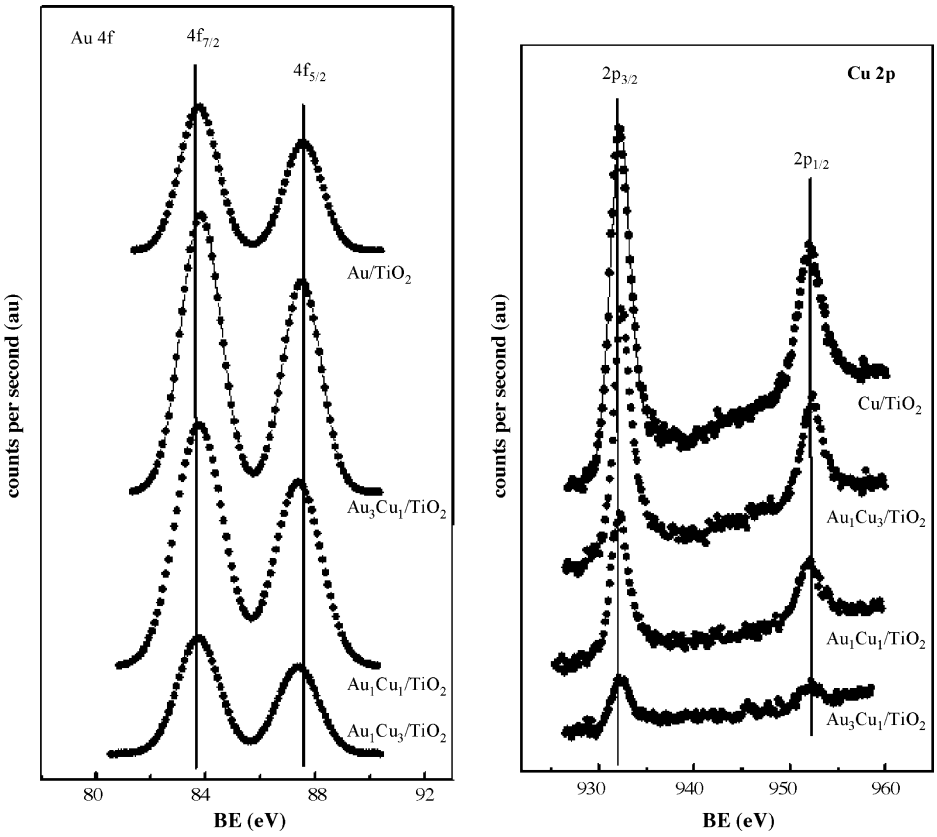

Fig. 9. X-ray photoelectron spectra recorded over 4%Cu/TiO_2, 4%Au/TiO_2 and 4%Au–Cu/TiO_2 catalysts.

occurring at the titania surface could modify the selectivity a blank experiment with pure support (TiO_2) was performed feeding propene oxide. No activity was observed for the TiO_2 alone. However, using a representative bimetallic catalysts (e.g. 4%Au_1Cu_3/TiO_2) that showed the highest activity for propene epoxidation, a conversion of 40% at the highest reaction temperature studied (653 K) was obtained. The main product was propanal (>70% of selectivity) together with other minor products such as acetone, acrolein and CO_x products. Thus, it is highly possible that the propanal obtained in our experiments is probably formed from the isomerization of the propene oxide. The values of propene conversion and selectivity to different products obtained over the various catalysts are shown in Table 2. Of all the samples tested, 4%Au/TiO_2 showed the lowest activity. In contrast, bimetallic catalysts were more active and propene conversion and selectivity towards propene oxide progressively increased as the copper content increased. The 4%Cu/TiO_2 sample was also active in propene epoxidation, as has been reported by Lambert and co-workers [31], but the catalytic performances of the 4%Au_1Cu_1/TiO_2 and 4%Au_1Cu_3/TiO_2 catalysts were superior than for the monometallic 4%Cu/TiO_2 sample. At a reaction temperature of 573 K (see Table 2), the 4%Cu/TiO_2 catalyst exhibited 2.4% of propene conversion, while the 4%Au/TiO_2, 4%Au_1Cu_1/TiO_2 and 4%Au_1Cu_3/TiO_2 exhibited 0.8, 3.9 and 4.3% of propene conversion, respectively. To compare the catalytic behaviour of monometallic gold catalysts (4%Au/TiO_2 and 0.5%Au/TiO_2), we performed an experiment in which we loaded 1.12 g of the 0.5%Au/TiO_2 catalyst instead of 0.140 g of the 4%Au/TiO_2 catalyst (eight times higher in order to obtain the same amount of gold). Propene con-

Table 2
Catalytic performance of Au–Cu/TiO_2 catalysts for propene epoxidation at 573 K

Catalyst	C_3H_6 (*X* %)	Selectivity (%)[a]					Rate (mmol g_{cat}^{-1} h^{-1})
		PO	PA	AC	ACR	CO_x	
4%Au/TiO_2	0.8	7.4	6.4	10.4	31.2	44.6	0.36
0.5%Au/TiO_2	1.4	10.5	8.6	11.0	24.6	43.1	0.63
4%Au_3Cu_1/TiO_2	1.9	12.4	12.2	11.3	21.4	42.7	0.86
4%Au_1Cu_1/TiO_2	3.9	23.6	10.1	11.5	18.5	36.3	1.78
4%Au_1Cu_3/TiO_2	4.3	26.3	12.7	13.2	15.6	32.2	1.96
4%Cu/TiO_2	2.4	12.6	10.3	11.1	24.0	42.0	1.09

Pressure: 1 atm, GHSV: 9000 h^{-1}, *X*: conversion of propene.
[a] PO: propene oxide, PA: propanal, AC: acetone, ACR: acrolein, CO_x (CO_2 and CO).

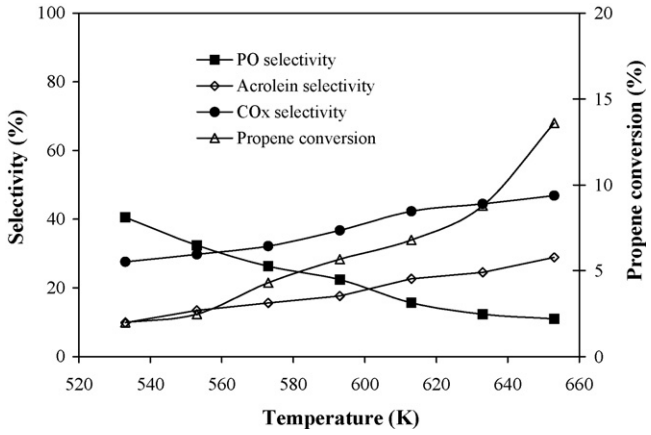

Fig. 10. Effect of temperature on the selectivity of the main products (left axis) and propene conversion (right axis) for the epoxidation of propene on $4\%Au_1Cu_3/TiO_2$ catalyst. Pressure: 1 atm, GHSV 9000 h^{-1}.

version was 1.4% for $0.5\%Au/TiO_2$. This conversion was higher than for the $4\%Au/TiO_2$ catalyst (0.89%) but lower than for the monometallic copper catalyst and bimetallic ones. Also, the bimetallic catalyst with the lowest Cu content, $4\%Au_3Cu_1/TiO_2$, exhibited the lowest activity of all bimetallic samples. The relative content of Au and Cu, therefore, appeared to play a determinant role in catalytic behaviour. There was evidence of alloy formation in the bimetallic samples. Our TPR experiments have also shown that the $4\%Au_1Cu_1/TiO_2$ and $4\%Au_1Cu_3/TiO_2$ catalysts, which have the highest conversion, also have an enhanced low temperature reduction peak in comparison with the other catalysts. If we take into account the metal particle sizes of our samples, the particular behaviour of the bimetallic catalysts may be due to alloying effects [32]. It has been suggested that, when copper is alloyed with gold, a net transfer of electrons is expected from copper to gold, thus, rendering copper deficient in electrons [33,34]. This has been confirmed by XPS analysis. Presumably, electron transfer also takes place from the reduced support to the metal clusters during the reaction. Because of electron transfer due to the interaction of nanosized clusters, the metal particles may become enriched in valence electron density, thereby altering the interaction of the active sites with the functional group and facilitating a partial transfer of electron density to the π^* orbital of the unsaturated bond of the olefin. This may also favour adsorption at cationic sites, thus, enhancing the electrophilic oxygen species and increasing the catalytic activity towards selective oxidation [35]. Moreover, the resulting weaker copper–gold bonds may favour the desorption of the reaction products, which may also explain the increase in catalytic activity observed for our bimetallic catalysts. Indeed, intimate metal-titania contacting appears to be essential for the production of partial oxidation capability. As the copper content increased, the metal particle size, determined by XRD, decreased from 27.1 nm for the $4\%Au/TiO_2$ catalyst to ca. 7.3 nm for the $4\%Au_1Cu_3/TiO_2$ catalyst, thus, increasing catalytic performance for the bimetallic samples. This size effect must also induce changes in the electronic properties of the metal nanoparticles [7].

Fig. 10 shows the temperature dependence on the catalytic performance of the $4\%Au_1Cu_3/TiO_2$ catalyst for the selective oxidation of propene by N_2O at 10 min of reaction. Propene conversion and selectivity to propene oxide were sensitive to the change in the reaction temperature. Propene conversion was 4.3% and selectivity was 26.3% in propene oxide for the $4\%Au_1Cu_3/TiO_2$ catalyst at 573 K (Fig. 10). At a reaction temperature of 533 K, conversion was 1.9% and selectivity to propene oxide was 40.5%. At a higher reaction temperature (653 K), conversion was 13.6% and selectivity to propene oxide was 10.9%.

Interestingly, in the range of reaction temperatures studied, propene oxide (PO) selectivity decreased but acrolein and CO_x selectivities generally increased as the reaction temperature increased. However, bimetallic catalysts always showed higher conversions and lower selectivity to CO_x than monometallic catalysts. These data provide further evidence of the different catalytic behaviour of alloy samples. Copper, therefore, had a marked effect on the catalytic properties of Au.

We should stress that some deactivation process was observed during the catalytic tests. According to previous studies, deactivation mainly occurs due to an irreversible adsorption of propene oxide on the catalyst surface, which undergoes further oligomerization, re-arrangment, cracking and coupling, etc. on acid sites [9]. However, the deactivation was completely reversible and the activity was completely restored after a regeneration procedure at 573 K under an oxygen/helium atmosphere.

4. Conclusions

Bimetallic Au–Cu particles supported over TiO_2 have been characterized and tested in the epoxidation of propene by N_2O. Structural studies by X-ray diffraction, XPS and transmission electron microscopy techniques demonstrated the existence of Au–Cu alloy particles. In addition, the alloy particle size decreased as the amount of copper in the catalysts increased. Cu can be used to modify the reactivity of Au with respect to the epoxidation of propene. Copper–gold bimetallic catalysts made up of alloy particles of about 5–15 nm were more active and selective towards propene oxide than monometallic Au or Cu samples supported over TiO_2. The most active catalysts consumed the largest amount of hydrogen at low temperature in TPR experiments, which suggests some spillover effect in the bimetallic catalysts. Both effects particle size and alloying are considered to play a determinant role in catalytic performance.

Acknowledgements

This research was sponsored by the Ministerio de Ciencia y Tecnología (Spain) under projects REN2002-04464-CO2-01, PETRI 95-0801.OP and by the Ministerio de Educación y Ciencia (Spain) under project CTQ2006-08196/PPQ. Part of this work was conducted at the Institut de Tècniques Energètiques (Universitat Politècnica de Catalunya) and supported by the Ministerio de Educación y Ciencia (Spain) under project ENE2006-06925/ALT.

References

[1] B. Hammer, J.K. Norskov, Nature 376 (1995) 238.
[2] M. Haruta, N. Yamada, T. Kobayashi, S. Iijima, J. Catal. 115 (1989) 301.
[3] M. Haruta, S. Tsubota, T. Kobayashi, H. Kageyama, M.J. Genet, B. Delmon, J. Catal. 144 (1993) 175.
[4] S.J. Ainsworth, Chem. Eng. News (1992) 9.
[5] T. Hayashi, K. Tanaka, M. Haruta, J. Catal. 178 (1998) 566.
[6] A.K. Sinha, S. Seelan, S. Tsubota, M. Haruta, Angew. Chem. Int. Ed. 43 (2004) 1546.
[7] M. Haruta, M. Daté, Appl. Catal., A 222 (2001) 427.
[8] T.A. Nijhuis, B.J. Huizinga, M. Makkee, J.A. Moulijn, Ind. Eng. Chem. Res. 38 (1999) 884.
[9] T.A. Nijhuis, T. Visser, B.M. Weckhuysen, J. Phys. Chem. B 109 (2005) 19309.
[10] O.P.H. Vaughan, G. Kyriakou, N. Macleod, M. Yikhov, R.M. Lambert, J. Catal. 236 (2005) 401.
[11] G. Ramis, G. Busca, F. Bregani, Gazz. Chim. Ital. 122 (1992) 79.
[12] V. Duma, D. Hönicke, J. Catal. 191 (2000) 93.
[13] S.J. Greg, K.S.W. Sing, Adsorption, Surface Area and Porosity, second ed., Academic Press, Londres, 1982.
[14] D. Briggs, M.P. Seah, Practical Surface Analysis: by Auger and X-ray Photoelectron Spectroscopy, John Wiley & Sons, New York, 1987.
[15] B. Coq, D. Tachon, F. Figuéras, G. Mabilon, M. Prigent, Appl. Catal. B 6 (1995) 271.
[16] D. Gelatt, H. Enrenreich, Phys Rev. B 10 (1974) 398.
[17] G. De, C.N.R. Rao, J. Phys. Chem. B 107 (2003) 1397.
[18] H. Chu, L. Yang, Q. Zhang, Y. Wang, J. Catal. 241 (2006) 225.
[19] S. Velu, K. Susuki, M. Okasaki, M.P. Kapoor, T. Osaki, F. Ohashi, J. Catal. 194 (2000) 373.
[20] L.J. Kundakovic, M.F. Stephanopoulos, Appl. Catal. A 171 (1998) 13.
[21] V. Ponec, Catal. Rev. Sci. Eng. 11 (1975) 41.
[22] G.C. Bond, Catal. Today 72 (2002) 5.
[23] S. Schimpf, M. Lucas, C. Mohr, U. Rodemerck, A. Brückenr, J. Radnik, H. Hofmeister, P. Claus, Catal. Today 72 (2005) 63.
[24] R.E. Kramer, H. Zuegg, J. Catal. 80 (1983) 446.
[25] F. Delannay, Characterization of Heterogeneous Catalysts, Decker, New York, 1984.
[26] X. Bao, M. Muhler, Th. Schedel-Niedrig, R. Schlöl, Phys. Rev. B 54 (1996) 2249.
[27] J.K.A. Clark, Chem. Rev. 75 (1975) 29.
[28] A.Q. Wang, J.H. Liu, S.D. Lin, T.S. Lin, C.Y. Mou, J. Catal. 233 (2005) 186.
[29] J.J. Pireau, M. Liehr, P.A. Thirty, J.P. Delrue, R. Caudano, Surf. Sci. 141 (1984) 221.
[30] B. Koslowski, H.G. Boyen, C. Wilderotter, G. Kästle, P. Ziemann, R. Wahrenberg, P. Oelhafen, Surf. Sci. 475 (2001) 1.
[31] O.P.H. Vaughan, G. Kryakou, N. Macleod, Mintcho Tikhov, R.M. Lambert, J. Catal. 236 (2005) 401.
[32] T. Akita, K. Tanaka, S. Tsuota, M. Haruta, J. Electron Microsc. 49 (2000) 657.
[33] D. Gelatt, H. Ehrenreich, Phys. Rev. B 10 (1974) 398.
[34] H. Over, G. Gilarowski, H. Niehus, Surf. Sci. Lett. 381 (1997) L619.
[35] M. Haruta, B.S. Uphade, S. Tsubota, A. Myamoto, Res. Chem. Intermed. 24 (1998) 329.